Simulation of Field-Effect Biosensors (BioFETs)

Thomas Windbacher *, Viktor Sverdlov *, Siegfried Selberherr *,
Clemens Heitzinger †, Norbert Mauser †, and Christian Ringhofer ‡

*Institute for Microelectronics, TU Wien, Gußhausstraße 27–29/E360, A–1040 Wien, Austria
Email: {Windbacher|Sverdlov|Selberherr}@iue.tuwien.ac.at
†Wolfgang Pauli Institute and Department of Mathematics, University of Vienna, Nordbergstrasse 15, A–1090 Wien, Austria
Email: {Clemens.Heitzinger|Norbert.Mauser}@univie.ac.at
‡Department of Mathematics, Arizona State University, Tempe, AZ 85287, USA
Email: Ringhofer@asu.edu

***Abstract*—In this paper a bottom-up approach for modeling field-effect Biosensors (BioFETs) is developed. Starting from the given positions of charged atoms, of a given molecule, the charge and the dipole moment of a single molecule are calculated. This charge and dipole moment are used to calculate the mean surface density and mean dipole moment at the biofunctionalized surface, which areintroduced into homogenized interface conditions linking the Angstrom-scale of the molecule with the micrometer-scale of the FET. By considering a single-stranded to double-stranded DNA reaction, we demonstrate the capability of a BioFET to detect a certain DNA and to resolve the DNA orientation.**

I. Introduction

Current technologies for detecting pathogens, tumor markers, and antigen-antibody complexes are expensive, complex, and time consuming. For instance, for detecting a certain DNA sequence with modern techniques [1], several processing steps are required. First, the biomolecule concentration has to be amplified by PCR (polymerase chain reaction) and labeled. The soluted biomolecules are analyzed by a microarray, in which every cell is able to detect a different type of biomolecule. After the chemical reaction took place, the cells are read using laser beams by an expensive microarray reader. Replacing the optical detection with an electrical signal detection used in BioFETs has several advantages. A BioFET is able to sense biomolecules without the need of PCR (polymerase chain reaction) and labeling [2], [3], [4], [5], so no optical reading device and laboratory is needed. Therefore BioFET microarrays can be used outdoors to control the spread of diseases and environmental pollution. Modern microelectronics allows to put a BioFET together with additional amplifying and analyzing circuits on the same chip without extra effort [6], thus enabling cheap mass production. Certain subsequences of a given organism's DNA can be identified as particular to it, thus DNA can provide a "species signature" enabling the unique identification of the organism. In this work we use a homogenized interface model [7], [8], [9], [10] to describe a BioFET. We demonstrate the generality of our approach to model a DNA hybridization reaction.

II. Simulation

The components of a BioFET are a semiconductor transducer, a dielectric layer, and a functionalized surface with immobilized biomolecule receptors, which are able to bind the desired biomolecule out of an aqueous solution (Figure 1). The n-MOS device has a gate length of one micrometer, so

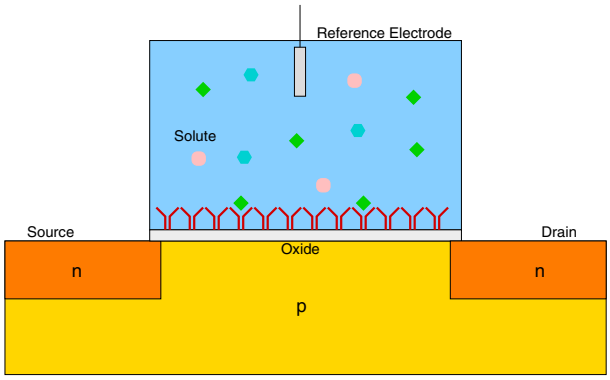

Fig. 1. Schematic diagram of a BioFET.

it is sufficient to apply the drift-diffusion model [11], [12]. The DNA hybridization requires salt to reduce the repulsive forces between the DNA strands. Higher salt concentrations cause faster hybridization but also less signal because of stronger screening. Sodium-chloride was taken into account when solving the Poisson-Boltzmann equation in the solute.

$$\epsilon_0 \nabla \cdot (\epsilon_{Ana} \nabla \psi(x,y)) = -\sum_{\sigma=\pm 1} \sigma \; q \; c_\sigma^\infty \; e^{-\sigma \frac{q}{k_B T}(\psi(x,y)-\psi_\mu)} \quad (1)$$

k_B is the Boltzmann's constant, T the temperature in Kelvin, and $\sigma = \pm 1$ for a 1:1 salt. ϵ_0 denotes the permittivity of vacuum, and q the elementary charge. ψ_μ is the contribution of the chemical potential. c_σ^∞ is the ion concentration in equilibrium, while $\epsilon_{Ana} \approx 80$ is the permittivity of water. The sum describes the carrier densities arising from the Boltzmann model. For a $1:1$ salt, like sodium-chloride, the expression

978-1-4244-1753-7/08/$25.00 ©2008 IEEE

given in (1) can be reformulated to:

$$\epsilon_0 \nabla \cdot (\epsilon_{Ana} \nabla \psi(x,y)) = 2\ q\ c_\sigma^\infty\ \sinh(\frac{q}{k_B T}(\psi(x,y) - \psi_\mu)). \tag{2}$$

The insulator surface charging due to the chemical reaction of H^+ and OH^- was modeled at $pH = 7$ with the site-binding model [13]:

$$Q_{Ox} = q\ N_S\ \frac{\frac{[H^+]_b}{K_a}\ e^{-\frac{q}{k_B T}\Psi(x,y)} - \frac{K_b}{[H^+]_b}\ e^{\frac{q}{k_B T}\Psi(x,y)}}{1 + \frac{[H^+]_b}{K_a}\ e^{-\frac{q}{k_B T}\Psi(x,y)} - \frac{K_b}{[H^+]_b}\ e^{\frac{q}{k_B T}\Psi(x,y)}}. \tag{3}$$

Q_{Ox} represents the surface charge due to chemical reactions with the analyte. N_S denotes the surface binding site density, while K_a and K_b are the equilibrium constants for charging the surface positively and negatively respectively. $[H^+]_b$ describes the positive hydrogen ion concentration of the bulk and is corrected to the activity of the hydrogen concentration by the $e^{\frac{q}{k_B T}\Psi(x,y)}$ terms. The equilibrium constants and the surface binding site densities for several materials are summarized in Table I [14]. Based on these values the surface charge density at different interfaces can be calculated from (3).

TABLE I
SHOWS THE PARAMETERS NEEDED FOR THE SITE-BINDING MODEL USING DIFFERENT MATERIALS.

Oxide	pK_a	pK_b	$N_S\ [cm^{-2}]$	Reference
SiO_2	-2	6	5.10^{14}	[15]
Al_2O_3	6	10	8.10^{14}	[15]
Ta_2O_5	2	4	10.10^{14}	[16]
Gold surface	4.5	4.5	1.10^{8}	[17]

If a charged molecule binds to the receptors, its charges change the potential near the transducer-surface and thus the conductance of the field-effect transistor channel. The change of the potential happens at the Angstrom-scale, while the device dimensions are in the micrometer-scale. It is crucial to have an appropriate model to describe the transducer-solution interface. The charges of the biomolecules which are shown in Figure 2 (geometry of the single-stranded DNA) and Figure 3 charge distribution, were modeled with a bottom-up approach [18]. Calculating the charge and dipole moment for a single molecule from a protein data bank [19] and relating these values to a surface density by choosing the mean distance between molecules allowed to link the Angstrom-scale of the molecules with the micrometer-scale of the FET.

The link between the gate oxide and the aqueous solution is realized by two interface conditions,

$$\epsilon_0 \epsilon_{Oxid}\ \partial_y \psi(0-,x) - \epsilon_0 \epsilon_{Ana}\ \partial_y \psi(0+,x) = -C(x), \tag{4}$$

$$\psi(0-,x) - \psi(0+,x) = -\frac{D_y(x)}{\epsilon_{Ana}\epsilon_0} \tag{5}$$

$\psi(0-)$ describes the potential in the oxide, while $\psi(0+)$ relates to the potential in the solute. The first equation describes the jump in the field due to the surface charge at the interface, while the second includes a dipole moment that causes a shift of the potential. The shift of the potential is taken into account by adjusting the potential in the analyte.

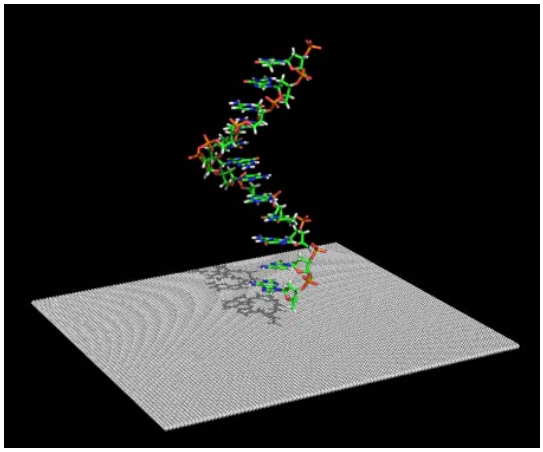

Fig. 2. The unbound single-stranded DNA at the surface of the dielectric.

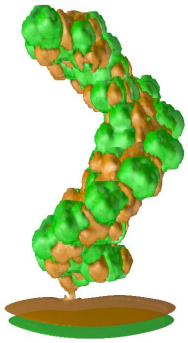

Fig. 3. Single-stranded DNA on the oxide surface. Two iso-surfaces for plus and minus $0.2\frac{k_B T}{q\mathring{A}^2}$ are shown.

Simulations were made for two surface concentrations of bound DNA equal to $10^{14}\mathrm{nm}^{-2}$ and $4.5 \cdot 10^{13}\mathrm{nm}^{-2}$. For each mean distance the output curves and potential profiles at different states were calculated. These states were the unprepared surface where no DNA is attached, the prepared but unbound state where single-stranded DNA is attached to

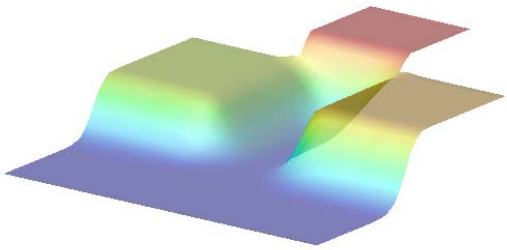

Fig. 4. Potential profile for double-stranded DNA perpendicular to surface for the whole device.

the surface, and the bound state when the single-stranded DNA has been hybridized to double-stranded DNA. In addition to these simulations, calculations for $0°$ (perpendicular to the surface) and $90°$ (parallel to the surface) were carried out. 100% binding efficency was assumed, thus resulting in optimal changes in characteristics and serving as outer bounds for real world situations. SiO_2 was chosen as dielectric. The potential at the reference electrode was set to 0.4V, setting the n-MOS to moderate inversion as proposed by [20].

III. Results

Figure 4 shows the potential profile in the BioFET including the solute. A cut of the potential profile through the middle of the device with and without the DNA is displayed in Figure 5. One can clearly see that, when negatively charged DNA is attached to the interface, the potential shifts upwards. This shift corresponds to a threshold voltage decrease which results in an increased resistance of the channel.

Figure 6 shows the influence of the DNA surface concentration on the output curves for single-stranded DNA (unbound state), while Figure 7 shows the influence of the DNA surface concentration on the output curves for double-stranded DNA (bound state). Comparison of these two figures shows that for higher concentration (smaller λ) the change in the output curves increases. The unbound state (single-stranded DNA) is negatively charged with 12 elementary charges, while the bound state (double-stranded DNA) possesses the double charge equal to 24 elementary charges. Therefore, the bound state of double-stranded DNA has got a larger negative surface charge which results in reduced current. This reduction is more pronounced for higher DNA concentration as it is seen in Figure 6 and Figure 7.

The output curves depending on the orientation of the DNA are depicted in Figure 8. It shows that the orientation perpendicular to the surface ($0°$) has the highest resistance in comparison to the other curves. Also the output curve with the DNA parallel to the surface has a higher resistance than the curve without dipole moment. This is due to the inhomogeneous charge distribution of the DNA and the dipole moment that is linked with it. The corresponding potential profiles in the middle of the device for different orientations are shown in Figure 9. For the orientation perpendicular ($0°$) to the surface the threshold voltage shift is the most negative one. While for the orientation parallel to the surface ($90°$) it is almost absent as compared to the case without dipole moment.

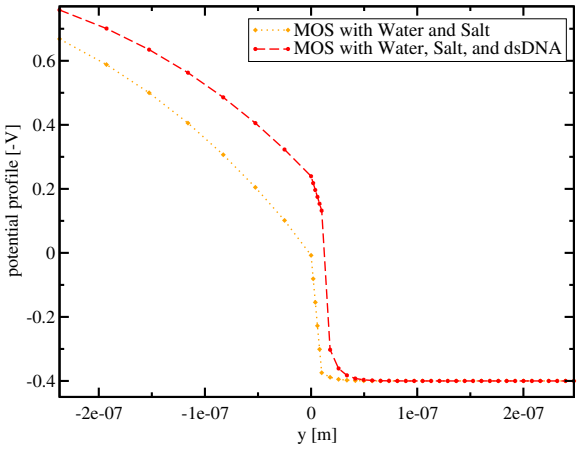

Fig. 5. Potential profile at the interface (from left to right: semiconductor, oxide, solute).

Over several years there has been a discussion if the orientation of the molecules attached to the surface has an effect on sensing [21], [22], [23], [24], [25]. Indeed biomolecules are inhomogeneously charged and possess therefore a dipole moment. The orientation of the biomolecule has to obey the energy minimization principle and there is an orientation that is preferred over others.

In [21], [22], [23], [24], [25] optical detection techniques were used. Although more study is needed, we mention that for optical detection it is more important to choose the linking molecule in a way that the reaction is not hindered by steric effects (receptors block each other) or the binding sites are blocked or even broken by the crosslinker. In the case of a BioFET, however, a field-effect as working principle is used. Thus it is important to have a linker that is as short as possible, to be close to the surface. To increase the signal to noise ratio, the linker should have as little charge as possible.

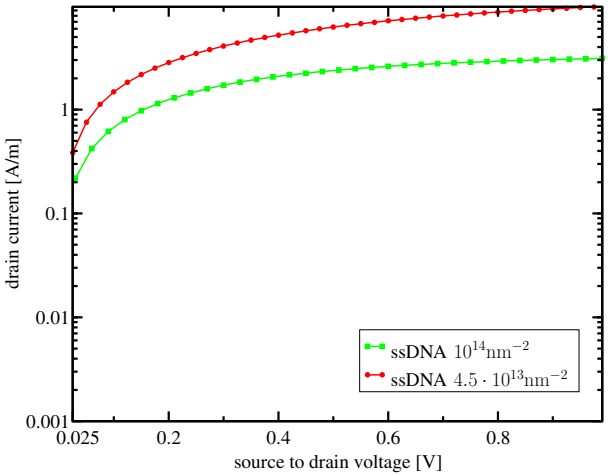

Fig. 6. Output characteristics of MOS before hybridization, for mean distance $10^{14}\mathrm{nm}^{-2}$ and $4.5 \cdot 10^{13}\mathrm{nm}^{-2}$ without dipole moment.

IV. Conclusion

The model shows a strong dependence on surface charges and is able to resolve DNA hybridization events. The bound state (double-stranded DNA) is negatively charged with 24 elementary charges, while the unbound state (single-stranded DNA) is negatively charged with 12 elementary charges. When hybridization has taken place and a double-stranded DNA is formed, reduced current is observed. Also the shift of the threshold voltage and output characteristics due to different molecule orientations ($0°$...perpendicular to surface, $90°$...lying flat on surface) can be detected. Therefore, the

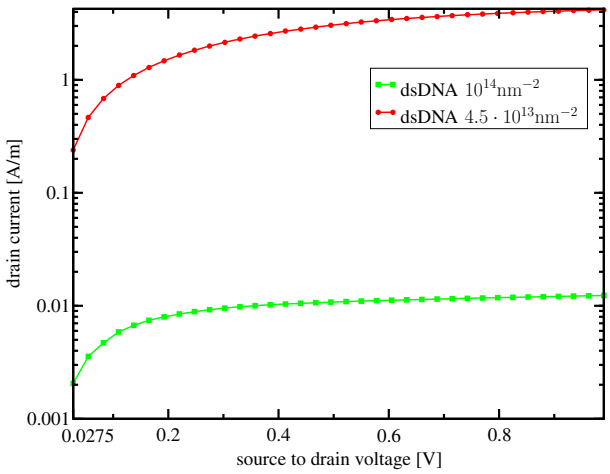

Fig. 7. Output characteristics of MOS after hybridization, for mean distance $10^{14}\mathrm{nm}^{-2}$ and $4.5 \cdot 10^{13}\mathrm{nm}^{-2}$ without dipole moment.

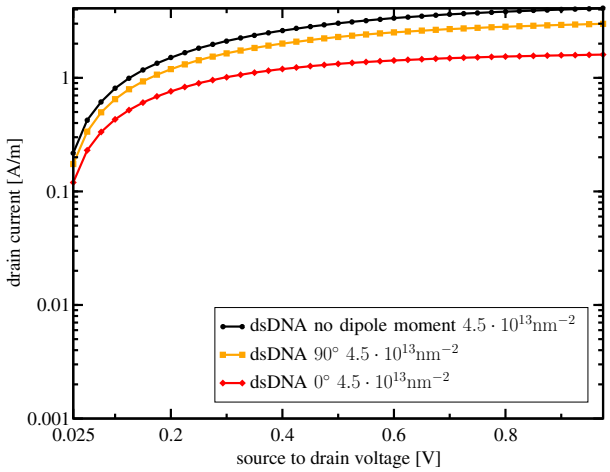

Fig. 8. Output characteristics of MOS after hybridization, for mean distance $4.5 \cdot 10^{13}\mathrm{nm}^{-2}$: without dipole moment, with $0°$, and $90°$.

model also describes a moderate shift in the threshold voltage depending on the molecule orientation related to the surface.

Acknowledgment

Help by Alexander Grill to setup a FET basis is gratefully acknowledged.

References

[1] M. C. Pirrung *Angew. Chem. Int. Ed.*, vol. 41, pp. 1276–1289, 2002.
[2] J.-i. Hahm and C. M. Lieber *Nano Letters*, vol. 4, no. 1, pp. 51–54, 2003.
[3] G. Zheng, F. Patolsky, Y. Cui, W. U. Wang, and C. M. Lieber *Nature Biotechnology*, vol. 23, no. 10, pp. 1294–1301, 2005.
[4] Z. Gao, A. Agarwal, A. D. Trigg, N. Singh, C. Fang, C. . Tung, Y. Fan, K. D. Buddharaju, and J. Kong *Analytical Chemistry*, vol. 79, no. 9, pp. 3291–3297, 2007.
[5] Y. Cui, Q. Wei, H. Park, and C. M. Lieber *Science*, vol. 293, no. 5533, pp. 1289–1292, 2001.
[6] M. J. Deen, "Highly Sensitive, Low-Cost Integrated Biosensors," in *SBCCI 2007: 20th Symposium on Integrated Circuits and System Design*, p. 1, 2007.
[7] C. Heitzinger, N. Mauser, and C. Ringhofer *SIAM J. Appl. Math.*, 2008. submitted.

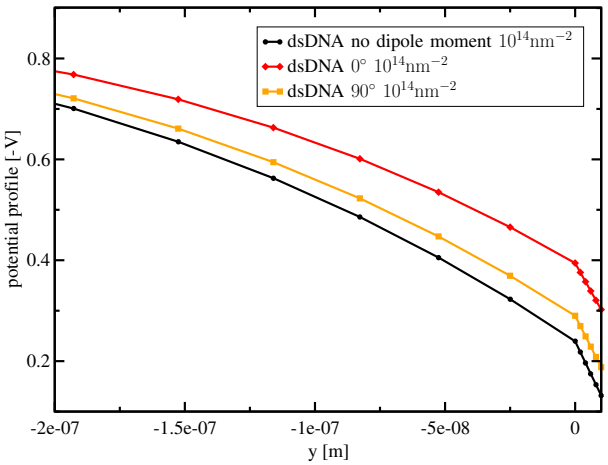

Fig. 9. Potential profile from semiconductor to oxide (left to right).

[8] C. Ringhofer and C. Heitzinger *ECS Transactions*, vol. 14, Aug. 2008. accepted.
[9] C. Heitzinger, R. Kennell, G. Klimeck, N. Mauser, M. McLennan, and C. Ringhofer *J. Phys.: Conf. Ser.*, vol. 107, pp. 012004/1–12, 2008.
[10] C. Heitzinger and G. Klimeck *J. Comput. Electron.*, vol. 6, no. 1-3, pp. 387–390, 2007.
[11] S. Selberherr, *Analysis and Simulation of Semiconductor Devices*, vol. Springer of *ISBN: 3-211-81800-6*. 1984.
[12] T.-W. Tang and M.-K. Ieong *IEEE Transactions on Computer-Aided Design of Integrated Circuits and Systems*, vol. 14, no. 11, pp. 1309–1315, 1995.
[13] M. W. Shinwari, M. J. Deen, and D. Landheer *Microelectronics Reliability*, Oct. 2006.
[14] D. Landheer, G. Aers, W. McKinnon, M. Deen, and J. Ranuárez *Journal of Applied Physics*, vol. 98, no. 4, pp. 044701–1 –044701–15, 2005.
[15] L. Bousse, *The Chemical Sensitivity of Electrolyte/Insulator/Silicon Structures*. PhD thesis, 1982.
[16] L. Bousse, S. Mostarshed, B. Van Der Shoot, N. F. De Rooij, P. Gimmel, and W. Gopel *Journal of Colloid and Interface Science*, vol. 147, no. 1, pp. 22–32, 1991.
[17] M. Giesbers, J. M. Kleijn, and M. A. Cohen Stuart *Journal of Colloid and Interface Science*, vol. 252, no. 1, pp. 138–148, 2002.
[18] A. Poghossian, A. Cherstvy, S. Ingebrandt, A. Offenhäusser, and M. J. Schöning *Sensors and Actuators, B: Chemical*, vol. 111-112, pp. 470–480, 2005.
[19] http://www.pdb.org.
[20] M. J. Deen, M. W. Shinwari, J. C. Ranuárez, and D. Landheer *Journal of Applied Physics*, vol. 100, no. 7, pp. 074703–1 –074703–8, 2006.
[21] S. W. Oh, J. D. Moon, H. J. Lim, S. Y. Park, T. Kim, J. Park, M. H. Han, M. Snyder, and E. Y. Choi *FASEB Journal*, vol. 19, no. 10, pp. 1335–1337, 2005.
[22] R. Wacker, H. Schroder, and C. M. Niemeyer *Analytical Biochemistry*, vol. 330, no. 2, pp. 281–287, 2004.
[23] W. Kusnezow, A. Jacob, A. Walijew, F. Diehl, and J. D. Hoheisel *Proteomics*, vol. 3, no. 3, pp. 254–264, 2003.
[24] P. Peluso, D. S. Wilson, D. Do, H. Tran, M. Venkatasubbaiah, D. Quincy, B. Heidecker, K. Poindexter, N. Tolani, M. Phelan, K. Witte, L. S. Jung, P. Wagner, and S. Nock *Analytical Biochemistry*, vol. 312, no. 2, pp. 113–124, 2003.
[25] J. Turkova *Journal of Chromatography B: Biomedical Sciences and Applications*, vol. 722, no. 1-2, pp. 11–31, 1999.